scientific reports

OPEN

Radiomics based on dual-energy CT virtual monoenergetic images to identify symptomatic carotid plaques: a multicenter study

Weiming Hu[1,2,7], Guihan Lin[1,7], Weiyue Chen[1], Jianhua Wu[1,2], Ting Zhao[1,2], Lei Xu[3,4], Xusheng Qian[5], Lin Shen[1], Zhihan Yan[3,4], Minjiang Chen[1], Shuiwei Xia[1], Chenying Lu[1], Jing Yang[6], Min Xu[1], Weiqian Chen[1,2] & Jiansong Ji[1✉]

This study aims to create a radiomics nomogram using dual-energy computed tomography (DECT) virtual monoenergetic images (VMI) to accurately identify symptomatic carotid plaques. Between January 2018 and May 2023, data from 416 patients were collected from two centers for retrospective analysis. Center 1 provided data for the training ($n=213$) and internal validation ($n=93$) sets, and center 2 supplied the external validation set ($n=110$). Plaques imaged at 40 keV, 70 keV, and 100 keV were outlined, and the selected radiomics features were used to establish the radiomics model. The classifier with the highest area under the curve (AUC) in the training set generated the radiomics score (Rad-Score). Logistic regression was used to identify risk factors and establish a clinical model. A radiomics nomogram integrating the Rad-score and clinical risk factors was constructed. The predictive performance was evaluated using receiver operating characteristic (ROC) analysis and decision curve analysis (DCA). Plaque ulceration and plaque burden are independent risk factors for symptomatic carotid plaques. The 40 + 70 keV radiomics model achieved excellent diagnostic performance, with an average AUC of 0.805 across all validation sets. Furthermore, the radiomics nomogram, integrating the Rad-score with clinical predictors, demonstrated robust diagnostic accuracy, with AUCs of 0.909, 0.850, and 0.804 in the training, internal validation, and external validation sets, respectively. DCA results suggested that the nomogram was clinically valuable. Our study developed and validated a DECT VMI-based radiomics nomogram for early identification of symptomatic carotid plaques, which can be used to assist clinical diagnosis and treatment decisions. The study introduces an innovative radiomics nomogram utilizing DECT VMI to discern symptomatic carotid plaques with high precision.

Keywords Dual-energy computed tomography, Symptomatic carotid plaque, Virtual monoenergetic images, Radiomics

Stroke is the third most prevalent cause of mortality and disability globally, with approximately seven million deaths attributed annually, a number that continues to escalate[1,2]. Approximately 20% of ischemic strokes are attributed to carotid atherosclerosis[3]. Symptomatic plaques are those that have caused symptoms such as transient ischemic attacks (TIA) or strokes and are closely linked to ischemic stroke risk[3,4]. Accurate early detection of these plaques is crucial for guiding timely interventions like medication, lifestyle changes, or surgery, which can prevent strokes and enhance patient outcomes and quality of life.

Computed tomography angiography (CTA) has the advantages of high spatial resolution and multi-plane reconstruction and is currently the main method for evaluating carotid atherosclerotic disease. Studies have

[1]Zhejiang Key Laboratory of Imaging and Interventional Medicine, Zhejiang Engineering Research Center of Interventional Medicine Engineering and Biotechnology, Key Laboratory of Precision Medicine of Lishui City, The Fifth Affiliated Hospital of Wenzhou Medical University, Lishui 323000, Zhejiang, China. [2]Department of Vascular Surgery, The Fifth Affiliated Hospital of Wenzhou Medical University, Lishui 323000, China. [3]Department of Radiology, The Second Affiliated Hospital of Wenzhou Medical University, Wenzhou 325000, China. [4]Wenzhou Key Laboratory of Structural and Functional Imaging, Wenzhou 325000, China. [5]Suzhou Institute of Biomedical Engineering and Technology, Chinese Academy of Sciences, Suzhou 215163, China. [6]Huiying Medical Technology Co., Ltd, Room A206, B2, Dongsheng Science and Technology Park, Haidian District, Beijing 100192, China. [7]Weiming Hu and Guihan Lin contributed equally to this work. ✉email: jjstcty@wmu.edu.cn

confirmed that CTA-identifiable plaque characteristics such as ulceration, thickness, and remodeling index are closely related to ischemic stroke risk[5]. Nevertheless, conventional evaluation methods depend on the expertise and experience of diagnosticians and need more specific objective quantitative indications. In recent years, dual-energy computed tomography (DECT) has become increasingly vital in evaluating carotid artery disease. DECT, utilizing different X-ray voltages, enhances imaging resolution beyond traditional CT; this enables accurate identification of susceptible calcified and lipid plaques, which is crucial for evaluating carotid stenosis[3,6–8]. Wang et al.[9] created a machine learning algorithm that merged DECT quantitative characteristics and clinical risk variables to detect symptomatic carotid plaques. They discovered that fat fraction and normalized iodine density were highly effective in predicting stroke events. Although the imaging capabilities of DECT have improved significantly, quantitative parameters still need to be measured manually. Therefore, automated and comprehensive methods must be developed to analyze complex imaging data of carotid artery plaques.

Radiomics utilizes advanced algorithms to transform detailed quantitative attributes from medical imaging into a high-dimensional, analyzable dataset. This process enhances clinical decision-making by delivering thorough, precise, and dependable data. Zheng et al. constructed a radiomics-based machine learning model using conventional CTA to identify patients with symptomatic carotid plaques. The outcomes demonstrated that the radiomics model much outperformed conventional evaluation techniques[10]. Recent research has begun to investigate the significant role of DECT-based radiomics in tumor detection, classification of diseased tissue subtypes, disease prognosis, and clinical decision-making[11,12]. Despite the successful use of DECT radiomics in oncology, its potential application in arterial plaque assessment remains largely unexplored.

The presented prediction model, constructed based on different energy level VMI radiomics analyses, is expected to significantly improve diagnostic efficiency and become an innovative and accurate assessment tool. Therefore, this study aimed to develop and validate a radiomics nomogram with DECT VMI to detect symptomatic carotid plaques.

Methods
Patient selection
This study conformed to the ethical standards established by institutional and national medical ethics committees, as well as the principles outlined in the 1964 Declaration of Helsinki and analogous guidelines. Approval for this observational study was granted by the Medical Ethics Committees of the Fifth (center 1) and Second (center 2) Affiliated Hospitals of Wenzhou Medical University (no. 2023- 796). Due to its retrospective design, the requirement for informed consent was waived by the medical ethics committees. Data were collected from patients diagnosed with and treated for extracranial carotid artery disease at center 1 from January 2018 to May 2023 and center 2 from January 2020 to May 2023. The study included clinical and radiographic data from patients diagnosed with atherosclerosis. The inclusion criteria were as follows: (1) age > 18 years; (2) carotid artery stenosis exceeding 30% as assessed by the North American Symptomatic Carotid Endarterectomy Trial (NASCET)[13]; (3) DECT CTA examination of the head and neck. Exclusion criteria were: (1) intracranial posterior circulation symptoms; (2) carotid artery stenosis due to radiotherapy, vasculitis, or other causes; (3) cardioembolic stroke; (4) history of carotid endarterectomy or stent implantation; (5) CTA indicates abnormal intracranial arterial lesions; (6) Presence of ulceration on the surface of the ascending aorta and/or significant aortic arch plaques that substantially affect the branches of the aortic arch; (7) poor image quality. Data from center 1 included 306 patients, divided into a training set of 213 and a validation set of 93, maintaining a 7:3 ratio. The data from center 2, comprising 110 patients, served as an independent external validation set. Figure 1 illustrates the patient recruitment flowchart.

Classification of cerebrovascular symptoms
Patients were classified into two groups based on their clinical presentations: symptomatic and asymptomatic. This classification depended on whether they had experienced an acute ischemic stroke (AIS) or a TIA in the anterior circulation area within the 2 weeks prior to undergoing the CTA examination. AIS is characterized by neurological impairment lasting over 24 h or by the identification of an acute cerebral infarction via imaging. TIA is described as a brief episode of neurological dysfunction due to diminished blood flow to specific brain or retinal regions, typically resolving within 24 h[14]. Study participants were each analyzed for a single carotid artery. For symptomatic patients, the carotid artery consistent with the symptoms was included. For asymptomatic patients, if both carotid arteries were eligible, the one with more severe stenosis was included.

Clinical data
Patient data that met the inclusion criteria were analyzed, including basic demographic information such as age, gender, and body mass index (BMI). Laboratory assessments comprised measurements of white blood cell count (WBC), triglycerides (TG), total cholesterol (TC), low-density lipoprotein cholesterol (LDL-C), high-density lipoprotein cholesterol (HDL-C), and blood glucose (BG). Documented vascular risk factors encompassed previous diagnoses of coronary artery disease (CAD), hyperlipidemia, diabetes, smoking behaviors, and hypertension.

Examination methods
Both centers utilized Somatom Force CT scanners (Siemens Healthineers, Germany) for head and neck CTA examinations. The contrast was achieved using Iopromide, with a concentration of 370 mg I/mL and a 30–40 mL volume, injected into the antecubital vein at 4–5 mL/s. DECT scanning parameters included a tube voltage of 150 kVp for tube A and 80 kVp for tube B, with automatic tube current modulation enabled. The rotation duration was set at 0.28 s, and the reconstruction layer thickness and spacing were 0.5 mm, with a pitch of 0.7. After transferring the data to the Siemens workstation (Syngo.via, version VB20A), three sets of VMI were generated
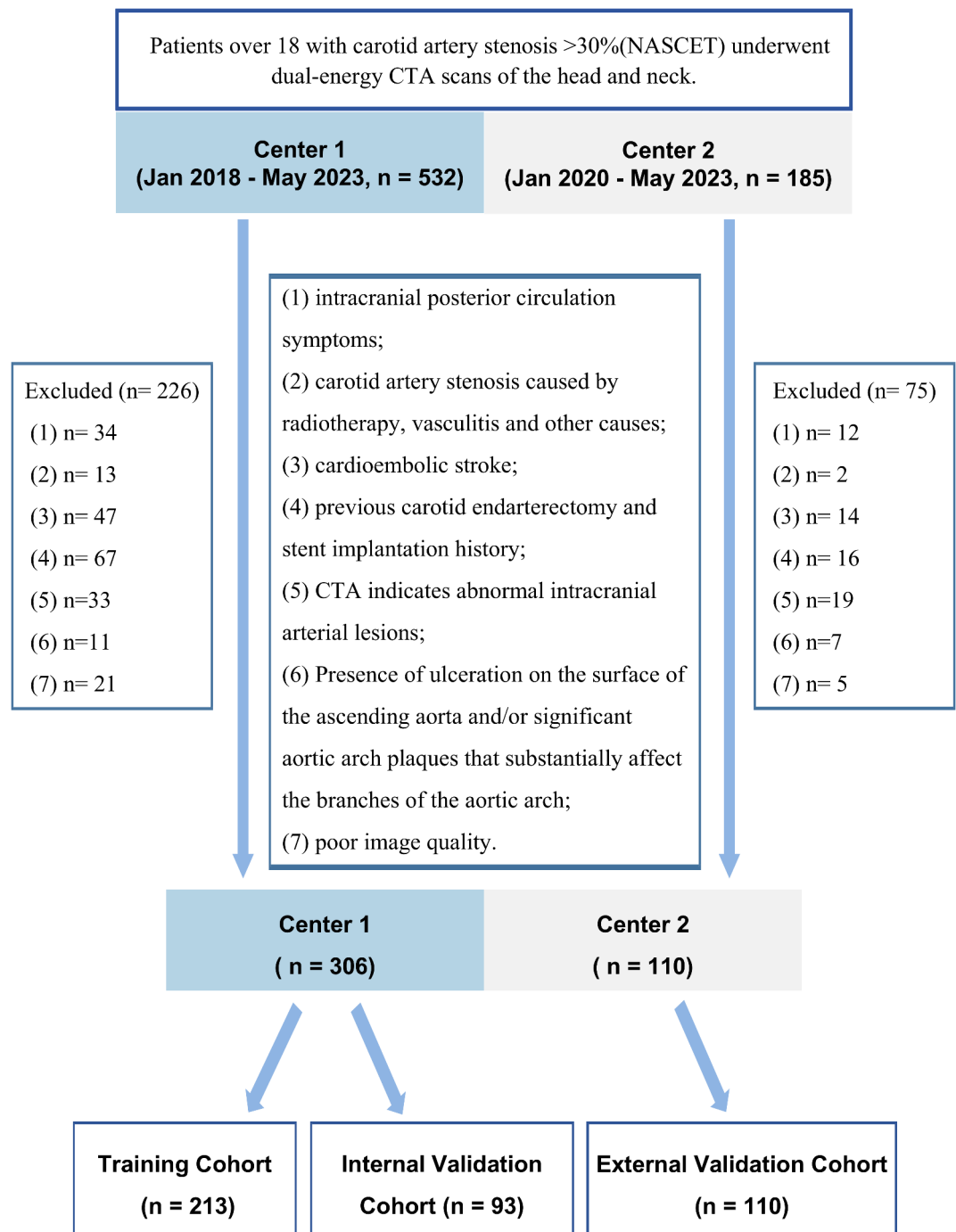
Patients over 18 with carotid artery stenosis >30%(NASCET) underwent dual-energy CTA scans of the head and neck.

Center 1
(Jan 2018 - May 2023, n = 532)

Center 2
(Jan 2020 - May 2023, n = 185)

(1) intracranial posterior circulation symptoms;

(2) carotid artery stenosis caused by radiotherapy, vasculitis and other causes;

(3) cardioembolic stroke;

(4) previous carotid endarterectomy and stent implantation history;

(5) CTA indicates abnormal intracranial arterial lesions;

(6) Presence of ulceration on the surface of the ascending aorta and/or significant aortic arch plaques that substantially affect the branches of the aortic arch;

(7) poor image quality.

Excluded (n= 226)

(1) n= 34

(2) n= 13

(3) n= 47

(4) n= 67

(5) n=33

(6) n=11

(7) n= 21

Excluded (n= 75)

(1) n= 12

(2) n= 2

(3) n= 14

(4) n= 16

(5) n=19

(6) n=7

(7) n= 5

Center 1
(n = 306)

Center 2
(n = 110)

Training Cohort
(n = 213)

Internal Validation
Cohort (n = 93)

External Validation Cohort
(n = 110)

Fig. 1. Flow diagram of the study population. *NASCET* North American Symptomatic Carotid Endarterectomy Trial.

at 40, 70, and 100 keV energy levels using the "Mono +" program. Measure the Fat Fraction of the plaque using the "Liver VNC" program. Details of the Fat Fraction measurement method can be found in Appendix E1.

CTA characteristics

Two radiologists with more than 5 years of experience in vascular imaging diagnosis recorded the conventional CTA characteristics of carotid artery plaques. Consultations were undertaken in circumstances where opinions differed to reach a consensus. The patient groups were hidden from both evaluators. Mild stenosis < 30%; moderate stenosis, between 30% and 69%; and severe stenosis 70-99%. Patients with mild stenosis were excluded from the study. The maximum thickness in the CTA's axial images was identified as the total plaque thickness. The maximum longitudinal extension of the plaque was called the plaque length. The presence of the contrast agent, more than 1.0 mm outside the artery lumen, indicated the presence of a plaque ulceration. A remodeling

index was employed to quantify positive remodeling. This index is calculated as the ratio of the vessel area at the site of maximal stenosis to an unaffected segment distally, with values exceeding 1 indicating positive remodeling. At the point of maximum stenosis, the plaque burden was determined using the formula ((1 − lumen area/vessel area) × 100)[15].

Plaque segmentation and feature extraction

Two independent radiologists used the Radcloud platform to mark the plaque outline layer-by-layer on each 40, 70, and 100 keV image to generate a volume of interest (VOI). After two weeks, 50 patients were randomly selected from center 1 and drawn independently by two radiologists to evaluate consistency between different observers. A total of 1688 radiomic characteristics were extracted from each VOI, including shape, first-order, texture features, and higher-order features derived specifically from wavelet transformations of the original images. Detailed descriptions of extracted features can be found in Appendix E2. The inter- and intraclass correlation coefficient (ICCs) were employed to assess the stability of the radiomic traits derived from the VOI. We considered the features with ICC value exceeded 0.8 as those with high stability and retained them for subsequent studies.

Feature selection and model construction

The univariate feature selection, variance analysis, and least absolute shrinkage and selection operator (LASSO) regression were used to identify high-dimensional features. Whereas univariate feature selection targets characteristics with a significance level of $P < 0.05$, variance analysis includes features if they exceed a threshold of 0.8. LASSO regression is utilized to derive the optimal set of features by screening for the best hyperparameters. Prior to model construction, z-score standardization was applied to the features to eliminate scale differences between them. Leveraging these characteristics, the support vector machine (SVM) algorithm was employed to create three distinct energy models (40 keV, 70 keV, and 100 keV) alongside four combined energy models (40 + 70 keV, 40 + 100 keV, 70 + 100 keV, and 40 + 70 + 100 keV) (Figs. S1 and S2). The model that exhibited the highest mean area under the curve (AUC) in the validation sets was designated the best-performing model. Results were then translated into a radiomics score (Rad-score). A radiomics nomogram was developed using a comprehensive method incorporating clinical risk variables with the Rad-score to enhance the prediction model's interpretability and accuracy. Figure 2 illustrates the radiomics procedure.

Statistical analysis

Statistical analyses were conducted using R (version 4.1.2, https://www.r-project.org/) and SPSS (version 26.0; IBM, Armonk, New York). The Shapiro-Wilk test was applied to evaluate the distribution of measurement data. For comparing groups with normally distributed data, as indicated by mean ± standard deviation, independent t-tests were employed. Conversely, the Mann–Whitney U test was utilized for groups with non-normally distributed data, which were described using medians and interquartile ranges. Categorical data, presented as frequencies, were analyzed using the chi-squared test. ROC curves were generated using the "pROC" package, and the Delong test was adopted to assess differences in the AUCs among various models. The "rms" package facilitated the creation of nomograms and calibration curves, while decision curve analysis (DCA) was performed with the "rmda" package. A significance threshold of $P < 0.05$ was established to identify statistically significant differences.

Results

Patient characteristics and clinical model construction

Statistical analyses revealed significant differences between the symptomatic and asymptomatic groups in the training set for variables including plaque ulceration, length, Lumen stenosis, severe stenosis, plaque burden, and Fat Fraction (all $P < 0.05$). Similarly, the internal validation set displayed significant variations in plaque ulceration, thickness, length, plaque burden, and Fat Fraction (all $P < 0.05$). In the external validation set, significant differences were also revealed in plaque ulceration, thickness, plaque burden, and Fat Fraction (all $P < 0.05$) (Table 1). Univariate and multivariate logistic regression analyses identified three independent risk factors for symptomatic carotid plaque: plaque ulceration (odds ratio [OR] = 12.307 [95% CI 4.060, 37.303], $P < 0.001$), plaque burden (OR = 1.057 [95% CI 1.020, 1.094], $P = 0.002$), and Fat Fraction (OR = 1.205 [95% CI 1.061, 1.369], $P = 0.004$) (Table S1). Based on these findings, a clinical model incorporating these factors yielded AUC values of 0.794, 0.757, and 0.743 across the training, internal validation, and external validation sets, respectively, as confirmed by ROC analysis (Table 3).

Feature selection and model construction

Each VOI shows a high degree of consistency in all the 1688 features extracted (all ICCs > 0.8). After feature selection, 13, 12, 10, 18, 14, 13, and 21 features were obtained from the three single (40 keV, 70 keV, and 100 keV) and four combined (40 + 70 keV, 40 + 100 keV, 70 + 100 keV, and 40 + 70 keV + 100 keV) VMI models, respectively (Table S2, Fig. S3). Figure 3 displays a heatmap of the correlation coefficients between the features. SVM was used to establish corresponding models for 40 keV, 70 keV, 100 keV, 40 + 70 keV, 40 + 100 keV, 70 + 100 keV, and 40 + 70 keV + 100 keV. The ROC curves constructed to evaluate the predictive capability of the models indicated that the AUC values ranged from 0.732 to 0.873 in the training set, 0.673 to 0.824 in the internal validation set, and 0.680 to 0.785 in the external validation set. Among the validation sets, the energy levels of 40 + 70 keV demonstrated the best diagnostic performance, with a mean AUC value of 0.805 (Table 2, Fig. S4).
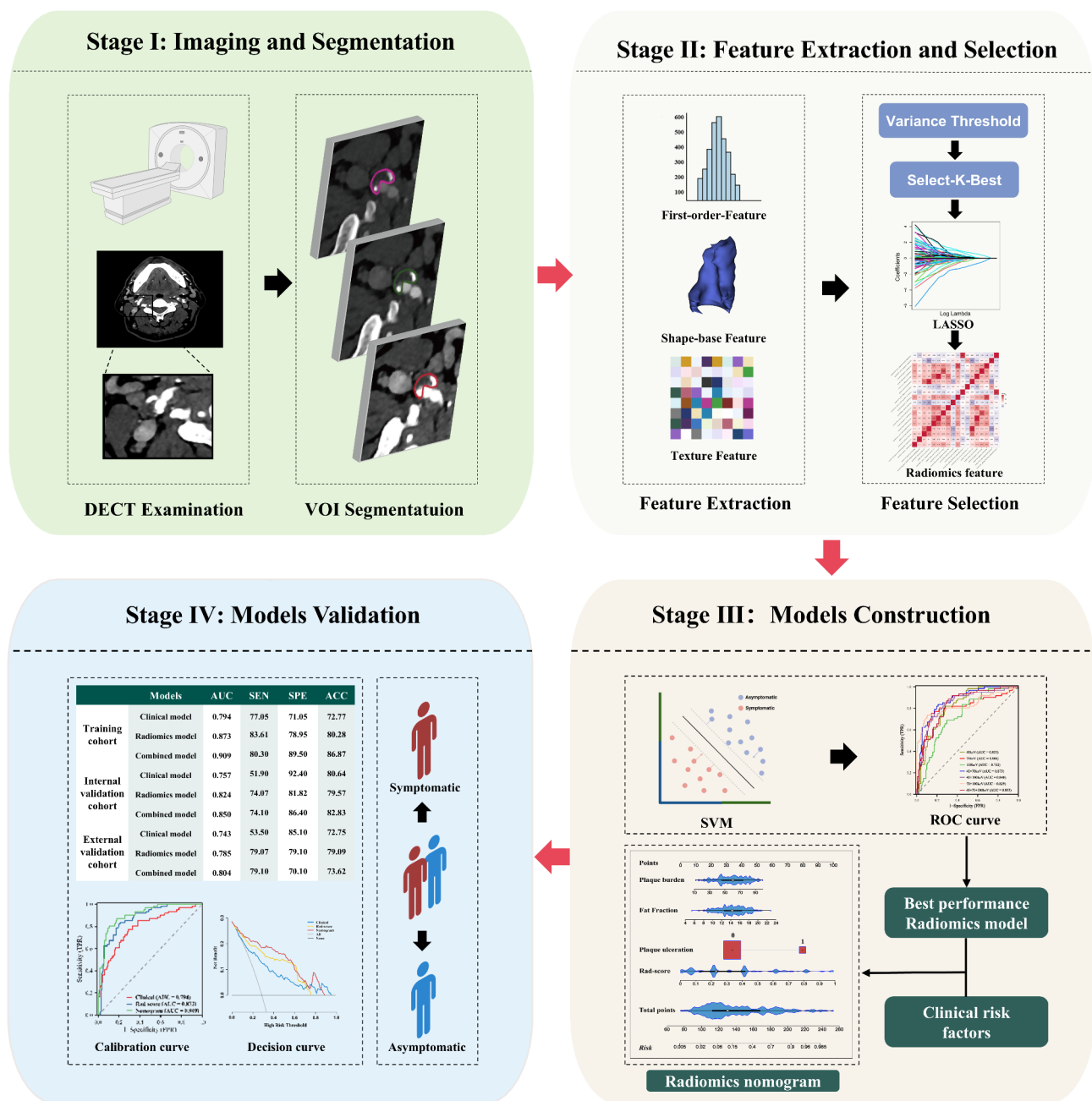
Fig. 2. The radiomics workflow. *DECT* dual-energy computed tomography, *VOI* volume of interest, *LASSO* the Least Absolute Shrinkage and Selection Operator, *SVM* support vector machine, *ROC* receiver operating characteristic curve.

Construction of radiomics nomogram

The radiomics nomogram was constructed based on plaque ulceration (OR = 14.497 [95% CI 4.111, 51.125]; $P < 0.001$), plaque burden (OR = 1.030 [95% CI 1.004, 1.056]; $P < 0.05$), Fat Fraction (OR = 1.188 [95% CI 1.030, 1.371], $P < 0.05$), and Rad-score (OR = 359.488 [95% CI 58.550, 2207.199]; $P < 0.001$) (Fig. 4, Table S3). The plaque signature and Rad-score can be calculated in clinical practice based on the evaluated characteristics. The probability of the predictive variable was used to construct a fraction that represents the first scale point at the top of the radiomics nomogram. After adding up the related prediction probabilities, the radiomics nomogram indicated the plaque risk at the bottom.

Evaluation of radiomics nomogram

The calibration curve (Fig. S5a–c) shows that the estimated probabilities from the radiomics nomogram closely fit the actual data. In the training set, the AUC, sensitivity, specificity, and accuracy of the radiomics nomogram were 0.909, 80.30%, 89.50%, and 86.87%, respectively, as indicated by the ROC results. Corresponding values

Characteristics	Training set (n = 213)			Internal validation set (n = 93)			External validation set (n = 110)		
	Symptomatic (n = 61)	Asymptomatic (n = 152)	p	Symptomatic (n = 27)	Asymptomatic (n = 66)	p	Symptomatic (n = 43)	Asymptomatic (n = 67)	p
Age, years*	73.13 ± 9.12	71.99 ± 8.55	0.404	72.70 ± 8.47	70.60 ± 8.25	0.280	72.86 ± 8.38	71.09 ± 9.13	0.308
Gender, Male (%)	47(77.0)	107(70.3)	0.327	19(70.3)	42(63.6)	0.535	34(79.1)	55(82.1)	0.694
BMI, kg/m²*	22.81 ± 3.87	23.27 ± 3.30	0.411	22.43 ± 3.25	23.39 ± 2.58	0.132	23.67 ± 3.99	24.33 ± 3.50	0.364
Smoking (%)	19(31.1)	30(19.7)	0.074	8(29.6)	12(18.2)	0.223	6(14.0)	11(16.4)	0.727
Diabetes (%)	17(27.9)	37(24.3)	0.593	6(22.2)	11(16.7)	0.529	17(39.5)	27(40.3)	0.936
Hypertension (%)	42(68.9)	100(65.8)	0.668	18(66.7)	43(65.2)	0.889	31(72.1)	50(74.6)	0.769
Hyperlipidemia (%)	4(6.6)	7(4.6)	0.561	4(14.8)	4(6.1)	0.172	5(11.6)	11(16.4)	0.487
CAD (%)	5(8.2)	14(9.2)	0.814	5(18.5)	8(12.1)	0.419	2(4.7)	14(20.9)	0.018
WBC, 10⁹/L*	6.20 (5.05,8.60)	6.55 (5.30,7.90)	0.968	6.55 (5.50,7.70)	6.80 (5.80,8.00)	0.512	6.43 (5.61,7.95)	6.75 (5.72,7.81)	0.849
TC, mmol/L*	3.94 (3.39,4.74)	4.26 (3.51,4.91)	0.205	4.32 (3.56,4.68)	4.53 (3.90,5.47)	0.111	3.73 (3.21,5.03)	4.11 (3.24,5.06)	0.472
TG, mmol/L*	1.12 (0.86,1.72)	1.26 (0.88,1.88)	0.350	1.22 (0.99,2.03)	1.52 (1.08,2.31)	0.166	1.33 (0.82,1.73)	1.23 (0.89,1.89)	0.579
HDL-C, mmol/L*	1.03 (0.82,1.21)	1.02 (0.88,1.23)	0.416	0.89 (0.77,1.11)	1.03 (0.88,1.21)	0.083	1.00 (0.84,1.24)	1.02 (0.78,1.40)	0.857
LDL-C, mmol/L*	1.89 (1.64,2.80)	2.24 (1.71,2.79)	0.220	2.33 (1.74,2.80)	2.20 (1.80,3.13)	0.469	2.26 (1.76,3.39)	2.54 (1.75,3.33)	0.752
BG, mmol/L*	5.8 (4.77,6.98)	5.53 (5.03,6.40)	0.822	5.56 (4.97,6.57)	5.74 (5.03,6.95)	0.559	6.84 (5.29,9.70)	6.40 (5.39,7.67)	0.622
Plaque ulceration (%)	20(32.8)	6(3.9)	< 0.001	8(29.6)	2(3.0)	< 0.001	10(23.3)	3(4.5)	0.003
Max plaque thickness, mm*	4.53 (3.33,5.57)	3.98 (3.12,4.96)	0.058	4.15 (3.72,5.33)	3.61 (3.16,4.88)	0.008	5.22 (4.17,6.34)	4.44 (3.73,5.42)	0.023
Max plaque length, mm*	16.00 (10.50,21.50)	12.00 (7.50,17.00)	0.001	16.00 (10.50,25.00)	12.00 (7.00,17.50)	0.034	12.60 (9.80,20.30)	14.70 (11.90,23.80)	0.157
Lumen stenosis (%)*	57.35 (44.09,69.76)	50.88 (36.20,59.52)	0.036	53.01 (43.52,62.39)	46.48 (40.91,56.58)	0.184	64.62 (55.37,70.90)	64.83 (53.83,69.85)	0.961
Severe stenosis (%)	15(24.6)	11(7.2)	< 0.001	4(14.8)	6(9.1)	0.419	11(25.6)	16(23.9)	0.840
Plaque burden*	67.67 ± 17.22	56.31 ± 18.00	< 0.001	66.19 ± 21.77	56.71 ± 18.89	0.038	68.65 ± 13.35	62.67 ± 10.89	0.012
PR (%)	58(95.1)	134(88.2)	0.125	24(88.9)	57(86.3)	0.742	43(100.0)	64(95.5)	0.159
Fat Fraction (%)*	15.17 ± 2.26	14.01 ± 3.14	0.003	15.12 ± 2.13	13.85 ± 1.88	0.006	15.43 ± 1.88	14.52 ± 2.32	0.035

Table 1. Clinical and CT morphological characteristics of patients in the training and two validation sets. *Values expressed as mean ± standard deviation or median (interquartile range) *BMI* body mass index, *CAD* coronary artery disease, *WBC* white blood cell, *TG* triglyceride, *TC* total cholestero, *HDL-C* high-density lipoprotein cholestero, *LDL-C* low-density lipoprotein cholestero, *BG* Blood glucose, *PR* positive remodeling.

in the internal validation set were 0.850, 74.10%, 86.40%, and 82.83%; in the external validation set, they were 0.804, 79.10%, 70.10%, and 73.62%, respectively (Fig. 5a–c; Table 3). The net benefit of the radiomics nomogram was greater than that of the clinical and radiomics models, as shown by the DCA findings (Fig. 5d–f). The AUCs of the clinical and radiomics models were compared with the radiomics nomogram using the DeLong test. The radiomics nomogram model performed significantly better in the training set than the clinical and radiomics model (P < 0.05). The radiomics nomogram showed a notable improvement over the clinical model in the internal validation set (P < 0.05). However, no statistically significant differences were found in the AUCs of the three models in the external validation set (P > 0.05) (Table S4).

Discussion

Atherosclerotic plaques in the carotid arteries are a significant risk factor for AIS. By developing personalized treatment plans and early intervention, the risk of cerebrovascular events can be effectively reduced, and patients' quality of life and prognosis can be improved. However, current approaches exhibit certain limitations in identifying symptomatic plaques, including the precise evaluation of plaque composition and determining plaque vulnerability. This study developed a VMI radiomics fusion model using DECT to facilitate the early detection of symptomatic carotid plaques. The results show that the model exhibits excellent performance and good generalization in predicting symptomatic carotid plaque.

CTA is now a standard procedure for assessing carotid artery disease. By transforming large medical imaging datasets into high-dimensional data and then extracting quantitative parameters for effective data mining and analysis, radiomics has recently been employed to evaluate lesion images thoroughly and accurately[16]. This technology overcomes the limits of subjective evaluation by utilizing quantitative image analysis techniques to greatly increase CT exams' diagnostic and predictive accuracy[17]. Predictive analysis of symptomatic carotid plaques has already been performed using a radiomics model based on traditional CTA. Shi et al.[18] retrospectively analyzed 167 patients with carotid plaques and constructed a radiomics model which performed slightly better in identifying symptomatic carotid plaques than conventional evaluation (AUC = 0.797 vs. AUC = 0.767). However, the performance of such models constructed using conventional carotid artery CTA is still sub-optimal. Conventional CTA images are susceptible to interference from calcification artifacts in structures surrounding calcified plaques; plaque composition and stability are difficult to accurately display and evaluate due to the complexity and overlap of their components. Currently, most of the studies on conventional
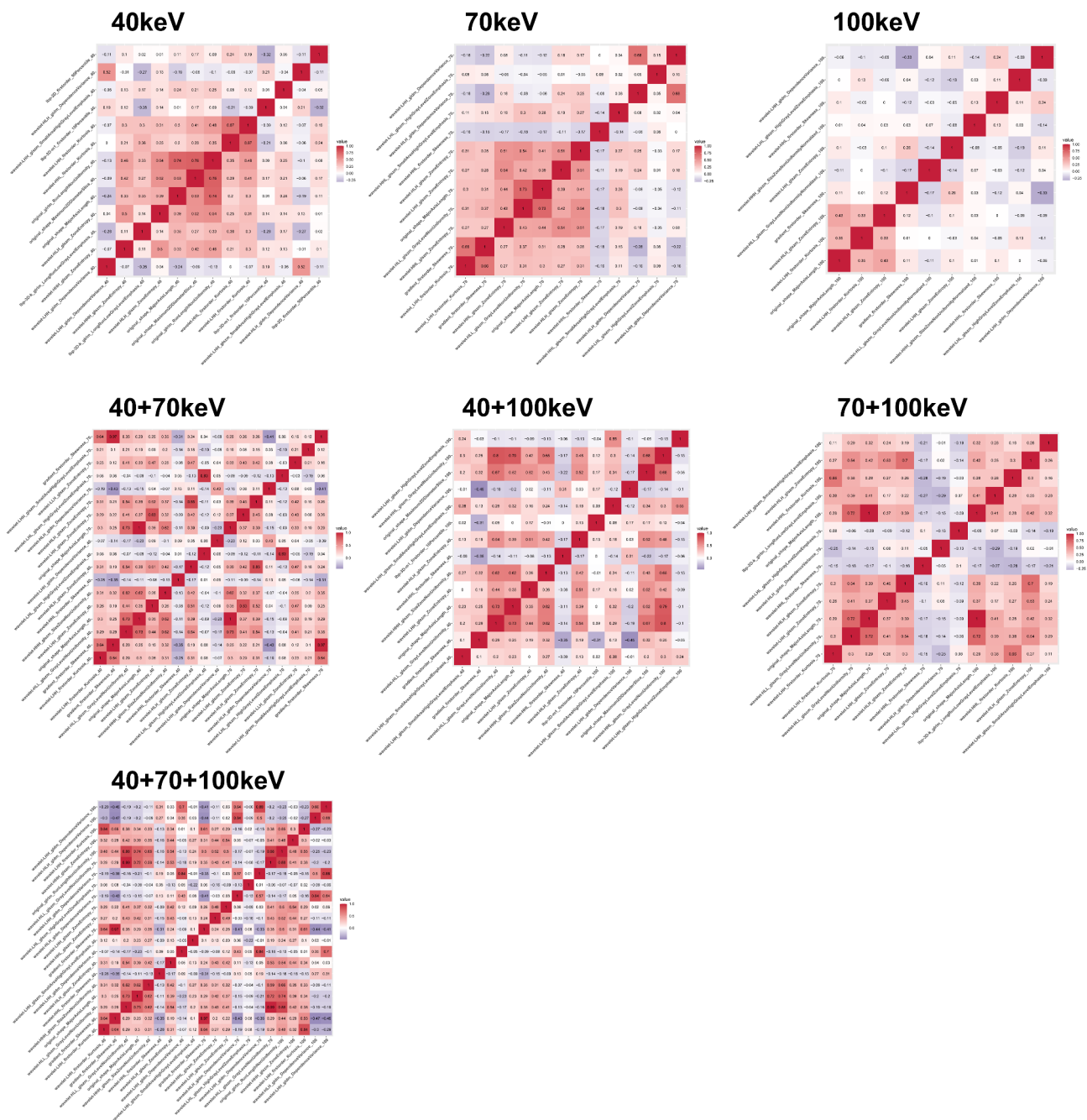
Fig. 3. The thermal diagram of radiomics feature correlation coefficients. Spearman correlation was performed between the selected features of the 40 keV, 70 keV, 100 keV, 40 + 70 keV, 40 + 100 keV, 70 + 100 keV, and 40 + 70 keV + 100 keV models. The thermal diagram displays the correlation coefficient between features. The thermal diagram is used for the prediction of selected characteristics of symptomatic carotid plaque. A positive correlation is shown by red, and a negative connection is shown by purple. Correlation strength is shown by color depth.

CTA-based radiomics for identifying symptomatic plaques are single-center and have limited sample sizes, which limits the generalization and wider applicability of their models. The multi-center nature of this study significantly enhances the generalizability of the presented radiomics model by improving the diversity and representativeness of its sample.

DECT generates multi-parameter information through linear combination and material separation technology to achieve quantitative evaluation of plaques, thus improving the accuracy of risk assessment[6]. It can enhance the attenuation of iodine at lower energy levels, replicate the image effects generated by monoenergetic X-rays, construct VMI images, and improve image contrast[19,20]. The study's findings demonstrate the efficacy of DECT VMI in locating symptomatic plaques. ROC analysis of the training, internal validation, and external

Model	Training set		Internal validation set		External validation set		Validation set	
	AUC (95% CI)	ACC	AUC (95% CI)	ACC	AUC (95% CI)	ACC	Average AUC	AverageACC
40 keV	0.822 (0.764–0.871)	75.12	0.749 (0.648–0.833)	70.97	0.735 (0.642–0.814)	70.91	0.742	70.94
70 keV	0.806 (0.747–0.857)	82.63	0.726 (0.624–0.814)	79.57	0.715 (0.621–0.797)	67.28	0.721	73.43
100 keV	0.732 (0.667–0.790)	69.95	0.673 (0.568–0.767)	66.67	0.680 (0.584–0.766)	67.28	0.677	66.98
40 + 70 keV	0.873 (0.820–0.914)	80.28	0.824 (0.731–0.895)	79.57	0.785 (0.696–0.858)	79.09	0.805	79.33
40 + 100 keV	0.840 (0.784–0.887)	76.53	0.675 (0.570–0.769)	67.75	0.748 (0.656–0.826)	69.09	0.712	68.42
70 + 100 keV	0.829 (0.772–0.877)	84.97	0.793 (0.696–0.870)	76.35	0.762 (0.671–0.838)	76.36	0.778	76.36
40 + 70 + 100 keV	0.833 (0.776–0.880)	74.65	0.781 (0.683–0.860)	76.34	0.768 (0.678–0.844)	77.23	0.775	76.79

Table 2. Diagnostic performance of various machine learning-based radiomics models. *AUC* area under the curve, *CI* confidence interval, *ACC* accuracy.

validation sets indicated that the DECT VMI model surpassed the radiomics models based on conventional DECT CTA images and traditional CTA assessment in prediction performance. The 40 keV low-energy VMI model outperformed the other models, achieving AUC values of 0.822, 0.749, and 0.735 in the training, internal validation, and external validation sets, respectively. The exceptional performance of this energy level is largely due to its proximity to the K edge of iodine (33 keV), which significantly enhances the contrast of blood vessels and improves the visibility of anatomical structures and plaques. Furthermore, the greatest attenuation difference between tissues occurs at low energy levels, which is advantageous for lesion detection[21]. Li et al. used DECT VMI at various energy levels to examine plaque pathology in patients having carotid endarterectomy; they discovered that DECT VMI at 40 keV had the highest accuracy in determining carotid plaque susceptibility, reaching 90.4%[22]. This study shows low-energy VMI can enhance diagnostic outcomes and maximize image quality. Conversely, the 100 keV high-energy VMI performance was the lowest of all the models. Although it has been demonstrated that high-energy VMI reduces foreign metal artifacts, contrast agent inflow, and beam hardening artifacts caused by plaque calcification in carotid artery imaging, poor overall performance occurs as the energy level increases due to a decrease in tissue contrast and iodine attenuation value[6,20,23]. Combining VMI at various energy levels increases the efficiency of the radiomics model in identifying symptomatic plaques, enriches the input characteristics, and provides consistent, high-quality data for radiomics analysis[19]. The 40 + 70 keV radiomics model demonstrated superior performance in this research, with AUC values of 0.873, 0.824, and 0.785 in the training, internal validation, and external validation sets, respectively.

According to the American Society of Neuroradiology and the European Society of Cardiology, the risk of stroke is significantly influenced by the composition and degree of stenosis of carotid artery plaques[24,25]. This study found significant differences in Fat Fraction, plaque burden and ulceration between symptomatic and asymptomatic patient groups. With respect to training, internal validation, and external validation sets, a clinical model that was built using these plaque features performed moderately (AUC: 0.794, 0.757, and 0.743, respectively). This result suggests that conventional plaque characterization is insufficient for reliably identifying symptomatic carotid plaques in clinical practice. In this study, we used DECT parameters to measure plaque Fat Fraction and found higher levels in the symptomatic group. This may relate to lipid core formation and enhanced inflammation, consistent with findings by Wang et al.[9], suggesting fat content as a key indicator of plaque stability. Plaque burden, a critical measure of stenosis and vascular remodeling, surpasses the importance of stenosis evaluation alone[26]. Symptomatic patients exhibited greater plaque burden, correlating with ischemic stroke presence and severity, consistent with previous research[27,28]. A significant plaque burden can lead to a hypoperfusion state, which is closely linked to a heightened risk of ischemic stroke. Plaque ulceration, indicating plaque vulnerability, increases stroke risk even in cases of mild stenosis and may result in neurological symptoms[29,30]. Ulceration is more often observed in symptomatic patients, reflecting its function as an indicator of plaque rupture and a predictor of stroke risk[31,32]. According to a meta-analysis, ulceration doubles the risk of ischemic stroke, most likely as a result of thrombus development at the ulcer site and hemodynamic alterations[33].

In order to address the above challenges, many studies have begun to explore radiomics nomograms that combine clinical and radiomics features to improve the model's predictive and diagnostic performance[5,34,35]. This comprehensive method not only increases the model's accuracy, but also makes the radiomics nomogram much easier for clinicians to use and comprehend, which helps medical professionals create more accurate treatment regimens[35]. The CTA-based radiomics nomogram developed by Liu et al. demonstrated high diagnostic accuracy in identifying high-risk carotid plaques[34]. To further enhance the accuracy of predicting symptomatic carotid artery lesions, we developed a radiomics nomogram in this study by integrating conventional clinical features with DECT VMI radiomics parameters. The model demonstrates strong predictive performance across the training, internal validation, and external validation sets, achieving AUC values of 0.909, 0.850, and 0.804 respectively. The radiomics nomogram shows great potential in clinical decision support due to its high accuracy and reliability. It aids in the early identification of high-risk patients and supports the implementation of tailored interventions to mitigate the risk of stroke.

This study has several limitations. First, its retrospective nature suggests that a prospective study is needed to assess the model more accurately. Second, the VOI was obtained through manual segmentation and has yet to be automated. Third, only one commonly used machine learning classifier was employed; the effectiveness of other classifiers in detecting symptomatic carotid plaques requires further investigation. Additionally, the study did not account for the potential influence of collateral circulation from the contralateral carotid artery
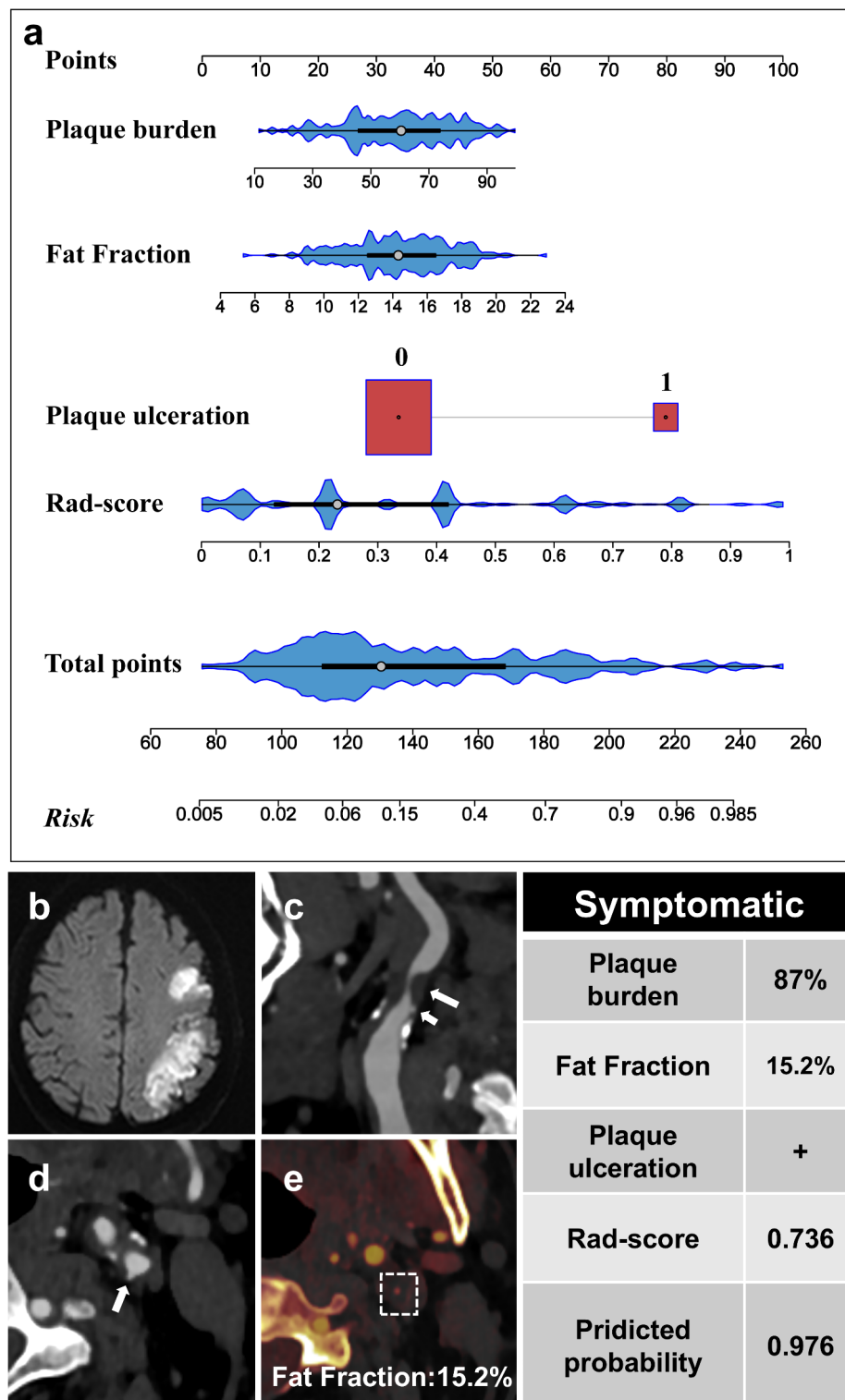
Fig. 4. (**a**) Radiomics nomogram. The radiomics nomogram, combining Fat Fraction, plaque burden, plaque ulceration, and Rad-score, was constructed in the training set. (**b–e**) For each below figure, a patient with symptomatic carotid plaque was selected as an example to illustrate the function of the radiomics nomogram. (**b**) Magnetic resonance diffusion-weighted imaging demonstrates a left-sided ischemic stroke in this patient. (**c**) Sagittal CTA reconstruction shows an internal carotid artery plaque (long arrow) and plaque ulceration (short arrow). (**d**) Axial CTA shows an internal carotid artery plaque near the internal carotid artery lumen with plaque ulceration (long arrow). (**e**) Using the "Liver VNC" program, measure the Fat Fraction of the plaque. Table showing predicted probability for this patient using radiomics nomogram.
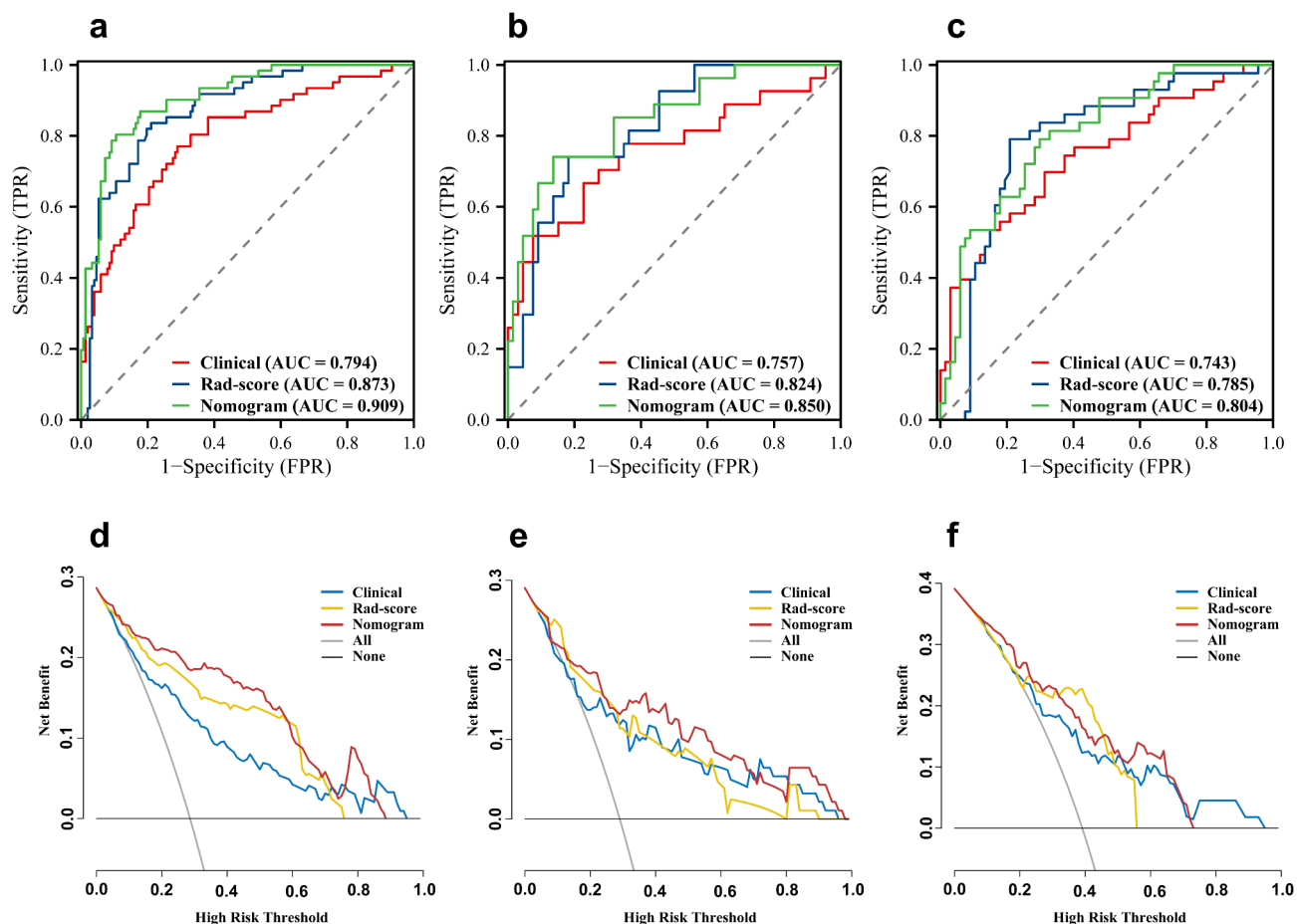
Fig. 5. ROC curves of clinical model, radiomics model, and radiomics nomogram in the training set (**a**), internal validation set (**b**), and external validation set (**c**). Decision curves of the training set (**d**), internal validation set (**e**), and external validation set (**f**). The y-axis represents net benefits; the x-axis represents threshold probability. The yellow, blue, and red lines represent the net advantages of the radiomics model, clinical model, and radiomics nomogram. The radiomics nomogram outperformed the clinical and radiomics models in terms of the total net benefit in distinguishing symptomatic carotid plaques. *AUC* area under the curve, *ROC* receiver operating characteristic.

	Models	AUC (95% CI)	SEN (%)	SPE (%)	ACC (%)
Training set	Clinical model	0.794 (0.734–0.847)	77.05	71.05	72.77
	Radiomics model	0.873 (0.820–0.914)	83.61	78.95	80.28
	Radiomics nomogram	0.909 (0.862–0.944)	80.30	89.50	86.87
Internal validation set	Clinical model	0.757 (0.657–0.840)	51.90	92.40	80.64
	Radiomics model	0.824 (0.731–0.895)	74.07	81.82	79.57
	Radiomics nomogram	0.850 (0.761–0.915)	74.10	86.40	82.83
External validation set	Clinical model	0.743 (0.651–0.822)	53.50	85.10	72.75
	Radiomics model	0.785 (0.696–0.858)	79.07	79.10	79.09
	Radiomics nomogram	0.804 (0.718–0.874)	79.10	70.10	73.62

Table 3. Diagnostic performance of clinical model, radiomics model and radiomics nomogram. *AUC* Area under the curve, *CI* confidence interval, *SEN* sensitivity, *SPE* specificity, *ACC* accuracy.

on hemodynamics, which limits the interpretation of results. Future studies should consider using advanced techniques, such as 4D flow MRI, to evaluate bilateral carotid arteries and further validate the findings.

Conclusions

In conclusion, this study utilized DECT VMI at various energy levels to develop a radiomics nomogram for identifying symptomatic carotid plaques. The model's outstanding predictive performance was confirmed through internal and external validation sets. Integrating conventional plaque features could further enhance recognition performance. In the future, it is expected to become a valuable tool for carotid plaque risk stratification and early intervention to prevent cerebrovascular events.

Data availability

The datasets generated during and/or analyzed during the current study are available from the corresponding author on reasonable request.

References

1. Wang, Y. et al. Burden of common neurologic diseases in Asian countries, 1990–2019: an analysis for the global burden of disease study 2019. *Neurology* **100**, e2141–e2154. https://doi.org/10.1212/wnl.0000000000207218 (2023).
2. Global national burden of stroke and its risk factors. 1990–2019: a systematic analysis for the global burden of disease study 2019. *Lancet Neurol.* **20**, 795–820. https://doi.org/10.1016/s1474-4422(21)00252-0 (2021).
3. Brinjikji, W. et al. Contemporary carotid imaging: from degree of stenosis to plaque vulnerability. *J. Neurosurg.* **124**, 27–42. https://doi.org/10.3171/2015.1.Jns142452 (2016).
4. Huang, L. X. et al. High-resolution magnetic resonance vessel wall imaging in ischemic stroke and carotid artery atherosclerotic stenosis: A review. *Heliyon* **10**, e27948. https://doi.org/10.1016/j.heliyon.2024.e27948 (2024).
5. Xia, H. et al. Predicting transient ischemic attack risk in patients with mild carotid stenosis using machine learning and CT radiomics. *Front. Neurol.* **14** https://doi.org/10.3389/fneur.2023.1105616 (2023).
6. Qu, H. et al. Dual energy computed tomography of internal carotid artery: A modified dual-energy algorithm for calcified plaque removal, compared with digital Subtraction angiography. *Front. Neurol.* **11**, 621202. https://doi.org/10.3389/fneur.2020.621202 (2020).
7. Saito, T. et al. Evaluation of cholesterol crystals in carotid plaque by dual energy computed tomography. *Neuroradiology* **65**, 979–982. https://doi.org/10.1007/s00234-023-03138-5 (2023).
8. Ebrahimian, S. et al. Spectral segmentation and radiomic features predict carotid stenosis and ipsilateral ischemic burden from DECT angiography. *Diagn. Interv. Radiol. (Ankara, Turkey).* **28**, 264–274. https://doi.org/10.5152/dir.2022.20842 (2022).
9. Wang, L. J. et al. Machine learning-based identification of symptomatic carotid atherosclerotic plaques with dual-energy computed tomography angiography. *J. Stroke Cerebrovasc. Dis. J. Natl. Stroke Assoc..* **32**, 107209. https://doi.org/10.1016/j.jstrokecerebrovasdis.2023.107209 (2023).
10. Dong, Z. et al. Radiomics versus conventional assessment to identify symptomatic participants at carotid computed tomography angiography. *Cerebrovasc. Dis.* **51**, 647–654. https://doi.org/10.1159/000522058 (2022).
11. Han, D. et al. Effect of radiomics from different virtual monochromatic images in dual-energy spectral CT on the WHO/ISUP classification of clear cell renal cell carcinoma. *Clin. Radiol.* **76**, 627. .e623-627.e629 (2021).
12. Bera, K., Braman, N., Gupta, A., Velcheti, V. & Madabhushi, A. Predicting cancer outcomes with radiomics and artificial intelligence in radiology. *Nat. Rev. Clin. Oncol.* **19**, 132–146. https://doi.org/10.1038/s41571-021-00560-7 (2022).
13. North American Symptomatic Carotid Endarterectomy Trial. Methods, patient characteristics, and progress. *Stroke* **22**, 711–720. https://doi.org/10.1161/01.str.22.6.711 (1991).
14. Tuna, M. A. & Rothwell, P. M. Diagnosis of non-consensus transient ischaemic attacks with focal, negative, and non-progressive symptoms: population-based validation by investigation and prognosis. *Lancet (London England).* **397**, 902–912. https://doi.org/10.1016/s0140-6736(20)31961-9 (2021).
15. Zhang, R. et al. Identification of high-risk carotid plaque with MRI-based radiomics and machine learning. *Eur. Radiol.* **31**, 3116–3126. https://doi.org/10.1007/s00330-020-07361-z (2021).
16. Mayerhoefer, M. E. et al. Introduction to radiomics. *J. Nucl. Med. Publ. Soc. Nuclear Med..* **61**, 488–495. https://doi.org/10.2967/jnumed.118.222893 (2020).
17. Polidori, T. et al. Radiomics applications in cardiac imaging: a comprehensive review. *Radiol. Med.* **128**, 922–933. https://doi.org/10.1007/s11547-023-01658-x (2023).
18. Shi, J. et al. Radiomics signatures of carotid plaque on computed tomography angiography: an approach to identify symptomatic plaques. *Clin. Neuroradiol.* **33**, 931–941. https://doi.org/10.1007/s00062-023-01289-9 (2023).
19. Leng, S., Yu, L., Fletcher, J. G. & McCollough, C. H. Maximizing iodine contrast-to-noise ratios in abdominal CT imaging through use of energy domain noise reduction and virtual monoenergetic dual-energy CT. *Radiology* **276**, 562–570. https://doi.org/10.1148/radiol.2015140857 (2015).
20. Zhao, J. et al. Optimal combination periprosthetic vasculature visualization and metal artifact reduction by spectral computed tomography using virtual monoenergetic images in total hip arthroplasty. *Insights Imaging.* **14**, 181. https://doi.org/10.1186/s13244-023-01533-3 (2023).
21. Lee, T. et al. Deep learning-based image reconstruction of 40-keV virtual monoenergetic images of dual-energy CT for the assessment of hypoenhancing hepatic metastasis. *Eur. Radiol.* **32**, 6407–6417. https://doi.org/10.1007/s00330-022-08728-0 (2022).
22. Li, Z. et al. Utility of dual-layer spectral detector CTA to characterize carotid atherosclerotic plaque components: an imaging-histopathology comparison in patients undergoing endarterectomy. *AJR Am. J. Roentgenol.* **218**, 517–525. https://doi.org/10.2214/ajr.21.26540 (2022).
23. Schoenbeck, D. et al. Imaging of intracranial hemorrhage in photon counting computed tomography using virtual monoenergetic images. *Neuroradiology* **66**, 729–736. https://doi.org/10.1007/s00234-024-03308-z (2024).
24. Aboyans, V. et al. ESC Guidelines on the Diagnosis and Treatment of Peripheral Arterial Diseases, in collaboration with the European Society for Vascular Surgery (ESVS): Document covering atherosclerotic disease of extracranial carotid and vertebral, mesenteric, renal, upper and lower extremity arteriesEndorsed by: the European Stroke Organization (ESO)The Task Force for the Diagnosis and Treatment of Peripheral Arterial Diseases of the European Society of Cardiology (ESC) and of the European Society for Vascular Surgery (ESVS). *Eur. Heart J.* **39**, 763–816. https://doi.org/10.1093/eurheartj/ehx095 (2018).
25. Saba, L., Guidelines from the ASNR Vessel Wall Imaging Study Group and Expert Consensus Recommendations of the American Society of Neuroradiology, et al. Carotid artery wall imaging: perspective and. *AJNR Am. J. Neuroradiol.* **39**, E9–e31. https://doi.org/10.3174/ajnr.A5488 (2018).

26. Cao, Y. et al. Atherosclerotic plaque burden of middle cerebral artery and extracranial carotid artery characterized by MRI in patients with acute ischemic stroke in China: association and clinical relevance. *Neurol. Res.* **39**, 344–350. https://doi.org/10.1080/01616412.2017.1281196 (2017).
27. Zhao, X. et al. Discriminating carotid atherosclerotic lesion severity by luminal stenosis and plaque burden: a comparison utilizing high-resolution magnetic resonance imaging at 3.0 Tesla. *Stroke* **42**, 347–353. https://doi.org/10.1161/strokeaha.110.597328 (2011).
28. Zhao, H. et al. Association of carotid atherosclerotic plaque features with acute ischemic stroke: a magnetic resonance imaging study. *Eur. J. Radiol.* **82**, e465–470. https://doi.org/10.1016/j.ejrad.2013.04.014 (2013).
29. Ballotta, E. et al. Carotid endarterectomy for symptomatic low-grade carotid stenosis. *J. Vasc. Surg.* **59**, 25–31. https://doi.org/10.1016/j.jvs.2013.06.079 (2014).
30. Kirkpatrick, J. Benefit of carotid endarterectomy in patients with symptomatic moderate or severe stenosis. *J. Insurance Med. (New York N. Y.).* **30**, 274–275 (1998).
31. Homburg, P. J. et al. Association between carotid artery plaque ulceration and plaque composition evaluated with multidetector CT angiography. *Stroke* **42**, 367–372. https://doi.org/10.1161/strokeaha.110.597369 (2011).
32. Benson, J. C. et al. MR imaging of carotid artery atherosclerosis: updated evidence on high-risk plaque features and emerging trends. *AJNR Am. J. Neuroradiol.* **44**, 880–888. https://doi.org/10.3174/ajnr.A7921 (2023).
33. Baradaran, H. et al. Association between carotid plaque features on CTA and cerebrovascular ischemia: A systematic review and meta-analysis. *AJNR Am. J. Neuroradiol.* **38**, 2321–2326. https://doi.org/10.3174/ajnr.A5436 (2017).
34. Liu, M. et al. Identification of vulnerable carotid plaque with CT-based radiomics nomogram. *Clin. Radiol.* **78**, e856–e863. https://doi.org/10.1016/j.crad.2023.07.018 (2023).
35. Lu, L. et al. Development and validation of a prognostic model for Post-Operative recurrence of pituitary adenomas. *Front. Oncol.* **12**, 882049. https://doi.org/10.3389/fonc.2022.882049 (2022).

Author contributions

W.M.H. participated in the study design, data collection, performed the statistical analysis, and drafted the manuscript. G.H.L. contributed to the study design and preparation, editing, and review of the manuscript. W.Y.C. and J.H.W. participated in the study design, contributed to quality control of data and algorithms, and editing and review of the manuscript. T.Z. and L.X. contributed to the preparation of the manuscript. X.S.Q. and J.Y. participated in data acquisition and analysis. L.S. and Z.Y. provided critical feedback on the manuscript. M.J.C., S.W.X., and C.Y.L. supervised the project and facilitated funding. M.X. and W.Q.C. contributed to manuscript revision. J.S.J. coordinated the study and finalized the manuscript. All authors read and approved the final manuscript.

Declarations

Competing interests

The authors declare no competing interests.

Additional information

Supplementary Information The online version contains supplementary material available at https://doi.org/10.1038/s41598-025-92855-3.

Correspondence and requests for materials should be addressed to J.J.

Reprints and permissions information is available at www.nature.com/reprints.

Publisher's note Springer Nature remains neutral with regard to jurisdictional claims in published maps and institutional affiliations.